



THE UNIVERSITY *of* EDINBURGH

Edinburgh Research Explorer

The formation of peak rings in large impact craters

Citation for published version:

Morgan, JV, Gulick, SPS, Bralower, T, Chenot, E, Christeson, G, Claeys, P, Cockell, C, Collins, GS, Coolen, MJL, Ferriere, L, Gebhardt, C, Goto, K, Jones, H, Kring, DA, Le Ber, E, Lofi, J, Long, X, Lowery, C, Mellett, C, Ocampo-Torres, R, Osinski, GR, Perez-Cruz, L, Pickersgill, A, Poelchau, M, Rae, A, Rasmussen, C, Rebolledo-Vieyra, M, Riller, U, Sato, H, Schmitt, DR, Smit, J, Tikoo, S, Tomioka, N, Urrutia-Fucugauchi, J, Whalen, M, Wittmann, A, Yamaguchi, KE & Zylberman, W 2016, 'The formation of peak rings in large impact craters', *Science*, vol. 354, no. 6314, pp. 878-882. <https://doi.org/10.1126/science.aah6561>

Digital Object Identifier (DOI):

[10.1126/science.aah6561](https://doi.org/10.1126/science.aah6561)

Link:

[Link to publication record in Edinburgh Research Explorer](#)

Document Version:

Version created as part of publication process; publisher's layout; not normally made publicly available

Published In:

Science

General rights

Copyright for the publications made accessible via the Edinburgh Research Explorer is retained by the author(s) and / or other copyright owners and it is a condition of accessing these publications that users recognise and abide by the legal requirements associated with these rights.

Take down policy

The University of Edinburgh has made every reasonable effort to ensure that Edinburgh Research Explorer content complies with UK legislation. If you believe that the public display of this file breaches copyright please contact openaccess@ed.ac.uk providing details, and we will remove access to the work immediately and investigate your claim.



GEOLOGY

The formation of peak rings in large impact craters

Joanna V. Morgan,^{1*} Sean P. S. Gulick,² Timothy Bralower,³ Elise Chenot,⁴ Gail Christeson,² Philippe Claeys,⁵ Charles Cockell,⁶ Gareth S. Collins,¹ Marco J. L. Coolen,⁷ Ludovic Ferrière,⁸ Catalina Gebhardt,⁹ Kazuhisa Goto,¹⁰ Heather Jones,³ David A. Kring,¹¹ Erwan Le Ber,¹² Johanna Lofi,¹³ Xiao Long,¹⁴ Christopher Lowery,² Claire Mellett,¹⁵ Rubén Ocampo-Torres,¹⁶ Gordon R. Osinski,^{17,18} Ligia Perez-Cruz,¹⁹ Annemarie Pickersgill,²⁰ Michael Poelchau,²¹ Auriol Rae,¹ Cornelia Rasmussen,²² Mario Rebolledo-Vieyra,²³ Ulrich Riller,²⁴ Honami Sato,²⁵ Douglas R. Schmitt,²⁶ Jan Smit,²⁷ Sonia Tikoo,²⁸ Naotaka Tomioka,²⁹ Jaime Urrutia-Fucugauchi,¹⁹ Michael Whalen,³⁰ Axel Wittmann,³¹ Kosei E. Yamaguchi,^{32,33} William Zylberman^{17,34}

Large impacts provide a mechanism for resurfacing planets through mixing near-surface rocks with deeper material. Central peaks are formed from the dynamic uplift of rocks during crater formation. As crater size increases, central peaks transition to peak rings. Without samples, debate surrounds the mechanics of peak-ring formation and their depth of origin. Chicxulub is the only known impact structure on Earth with an unequivocal peak ring, but it is buried and only accessible through drilling. Expedition 364 sampled the Chicxulub peak ring, which we found was formed from uplifted, fractured, shocked, felsic basement rocks. The peak-ring rocks are cross-cut by dikes and shear zones and have an unusually low density and seismic velocity. Large impacts therefore generate vertical fluxes and increase porosity in planetary crust.

Impacts of asteroids and comets play a major role in planetary evolution by fracturing upper-crustal lithologies, excavating and ejecting material from the impact site, producing melt pools, and uplifting and exposing subsurface rocks. The uplift of material during impact cratering rejuvenates planetary surfaces with deeper material. Complex impact craters on rocky planetary bodies possess a central peak or a ring of peaks internal to the crater rim, and the craters with these features are termed central-peak and peak-ring craters, respectively (1). Most known peak-ring craters occur on planetary bodies other than Earth, prohibiting assessment of their physical state and depth of origin. Here, we address the question of how peak rings are formed, using geophysical data, numerical simulations, and samples of the Chicxulub peak ring obtained in a joint drilling expedition by the International Ocean Discovery Program (IODP) and International Continental Scientific Drilling Program (ICDP).

Upon impact, a transient cavity is initially formed, which then collapses to produce a final crater that is both shallower and wider than the transient cavity (1). Dynamic uplift of rocks during the collapse of the transient cavity in the early stages of crater formation (Fig. 1, B and C) likely forms central peaks (2). The dynamic collapse model of peak-ring formation attributes the origin of peak rings to the collapse of over-heightened central peaks (3). The observational evidence for this model is most obvious on Venus, where central peaks gradually evolve into

peak rings with increasing crater size (4). The peak-ring-diameter-to-crater-rim-diameter ratio increases with crater size on Venus but does not get much larger than ~0.5. The lack of any further increase in this ratio led to the suggestion that in larger craters, the outward collapse of peak-ring material is halted when it meets the collapsing transient cavity rim (4).

A different concept for peak-ring formation—the nested melt-cavity hypothesis—evolved from observations of peak-ring craters on the Moon and Mercury (5–7). This alternative hypothesis envisions that the uppermost central uplift is melted during impact, and an attenuated central uplift remains below the impact melt sheet and does not overshoot the crater floor during the modification stage. Hence, in contrast to the dynamic collapse model (Fig. 1), this nested melt-cavity hypothesis would not predict outward thrusting of uplifted rocks above the collapsed transient cavity rim material. The origin and shock state of rocks that form a peak ring are less clear in the nested melt-cavity hypothesis because they have not been evaluated with numerical simulations. Head, however, postulated that material in the outer margin of the melt cavity forms the peak ring and therefore should be close to melting (6). This requires shock pressures of just below 60 GPa. In contrast, Baker *et al.* propose that peak rings are formed from inwardly slumped rotated blocks of transient cavity rim material originating at shallow depths and thus should have experienced lower average shock pressures than simulated in the dynamic collapse model (7).

The transition from central-peak to peak-ring craters with increasing crater size scales inversely with gravity (1), suggesting that the same transition diameter of ~30 km found on Venus (4) should also hold for Earth, and that craters >30 km in diameter should possess a peak ring. Craters on Earth often display internal ring-like structures, but complications and uncertainties owing to target heterogeneity, erosion, and sedimentation make it difficult to distinguish peak rings that are genetically linked to their extraterrestrial counterparts (8, 9). Seismic reflection data across the ~200-km-diameter Chicxulub multi-ring impact structure revealed it to be the

¹Department of Earth Science and Engineering, Imperial College London, SW7 2AZ, UK. ²Institute for Geophysics, Jackson School of Geosciences, University of Texas at Austin, TX 78758-4445, USA. ³Department of Geosciences, Pennsylvania State University, University Park, PA 16802, USA. ⁴Biogéosciences Laboratory, UMR 6282 CNRS, Université de Bourgogne-Franche Comté, Dijon 21000, France. ⁵Analytical, Environmental and Geo-Chemistry, Vrije Universiteit Brussel, Pleinlaan 2, Brussels 1050, Belgium. ⁶Centre for Astrobiology, School of Physics and Astronomy, University of Edinburgh, Edinburgh EH9 3FD, UK. ⁷Department of Chemistry, WA-Organic and Isotope Geochemistry Centre (WA-OIGC), Curtin University, Bentley, WA 6102, Australia. ⁸Natural History Museum, Burghing 7, 1010 Vienna, Austria. ⁹Alfred Wegener Institute Helmholtz Centre of Polar and Marine Research, Bremerhaven, 27568, Germany. ¹⁰Tohoku University, International Research Institute of Disaster Science, Aoba 468-1 E303, Sendai 980-0845, Japan. ¹¹Lunar and Planetary Institute, 3600 Bay Area Boulevard, Houston, TX 77058, USA. ¹²Department of Geology, University of Leicester, Leicester, LE1 7RH, UK. ¹³Géosciences Montpellier, Université de Montpellier, 34095 Montpellier Cedex 05, France. ¹⁴China University of Geosciences (Wuhan), School of Earth Sciences, Planetary Science Institute, 388 Lumo Rd. Hongshan Dist., China. ¹⁵British Geological Survey, The Lyell Centre, Research Avenue South, Edinburgh, EH14 4AP, UK. ¹⁶Groupe de Physico-Chimie de l'Atmosphère, L'Institut de Chimie et Procédés pour l'Energie, l'Environnement et la Santé (ICPEES), UMR 7515 Université de Strasbourg-CNRS 1 rue Blessig, 67000 Strasbourg, France. ¹⁷Centre for Planetary Science and Exploration and Department of Earth Sciences, University of Western Ontario, London, ON, N6A 5B7, Canada. ¹⁸Department of Physics and Astronomy, University of Western Ontario, London, ON, N6A 5B7, Canada. ¹⁹Instituto de Geofísica, Universidad Nacional Autónoma de México, C. D. Universitaria, Coyoacán Ciudad de México, C. P. 04510, México. ²⁰School of Geographical and Earth Sciences, University of Glasgow, Gregory, Lilybank Gardens, Glasgow, G12 8QQ, UK. ²¹University of Freiburg, Geology, Albertstraße 23b, Freiburg, 79104, Germany. ²²University of Utah, Department of Geology and Geophysics, 115 S 1460 E (FASB), Salt Lake City, UT 84112, USA. ²³Unidad de Ciencias del Agua, Centro de Investigación, Científica de Yucatán, A.C., Cancún, Quintana Roo, C.P. 77500, México. ²⁴Institut für Geologie, Universität Hamburg, Bundesstrasse 55, Hamburg, 20146, Germany. ²⁵Japan Agency for Marine-Earth Science and Technology, 2-15, Natsushima-cho, Yokosuka-city, Kanagawa, 237-0061, Japan. ²⁶Department of Physics, University of Alberta, Edmonton, Alberta, T6G 2E1, Canada. ²⁷Faculty of Earth and Life Sciences (FALW), Vrije Universiteit Amsterdam, de Boelelaan 1085, Amsterdam, 1018HV, Netherlands. ²⁸Rutgers University New Brunswick, Earth and Planetary Sciences, Piscataway Township, NJ 08854, USA. ²⁹Kochi Institute for Core Sample Research, Japan Agency for Marine-Earth Science and Technology, 200 Monobe Otsu, Nankoku, Kochi, 783-8502, Japan. ³⁰Department of Geosciences, University of Alaska Fairbanks, 900 Yukon Drive, Fairbanks, AK 99775, USA. ³¹Arizona State University, LeRoy Eyring Center for Solid State Science, Physical Sciences, Tempe, AZ 85287-1704, USA. ³²Department of Chemistry, Toho University, Funabashi, Chiba 274-8510, Japan. ³³NASA Astrobiology Institute, USA. ³⁴Aix Marseille Université, CNRS, Institut pour la Recherche et le Développement, Coll France, CEREGE, Aix-en-Provence, France.

*Corresponding author. Email: jmorgan@imperial.ac.uk

only terrestrial crater with an unequivocal and intact peak ring, with the same morphological structure as peak-ring craters on Venus, Mercury, the Moon, and other rocky bodies (10–14). These seismic data and previous drilling also revealed a terrace zone formed from slump blocks of Mesozoic sedimentary rocks, with the innermost blocks lying directly underneath or close to the outer edge of the peak ring (Fig. 1G). This observation supported the idea that peak rings in larger craters could be created through the interaction of two collapse regimes, with the peak-ring rocks being formed from uplifted crustal basement

that had collapsed outward and been emplaced above the collapsed transient cavity rim (15).

Numerical shock-physics simulations (Fig. 1) are consistent with the dynamic collapse model in that they reproduce this mode of peak-ring formation as well as other crater features, such as the observed mantle uplift and terrace zone (16–20). For the simulation in Fig. 1, we used well and geophysical data to construct the pre-impact target, which is composed of a 33-km-thick crust with ~3 km of sedimentary rocks above the basement (21). We tracked the material that eventually forms the Chicxulub peak ring and

show that it originates from mid-crustal basement (8- to 10-km depth) that is shocked to pressures >10 GPa (Fig. 1A). The peak-ring rocks first move outward and upward as the initial transient cavity forms (Fig. 1B), then progress inward to form part of the zone of central uplift (Fig. 1C), and finally collapse outward to be emplaced above collapsed transient cavity rim material composed of sedimentary rocks (Fig. 1C, light gray) that were originally between 0- and 3-km depth (Fig. 1, D to F). The dynamic collapse model therefore predicts that the Chicxulub peak ring is formed from uplifted crystalline basement rocks. Structural data

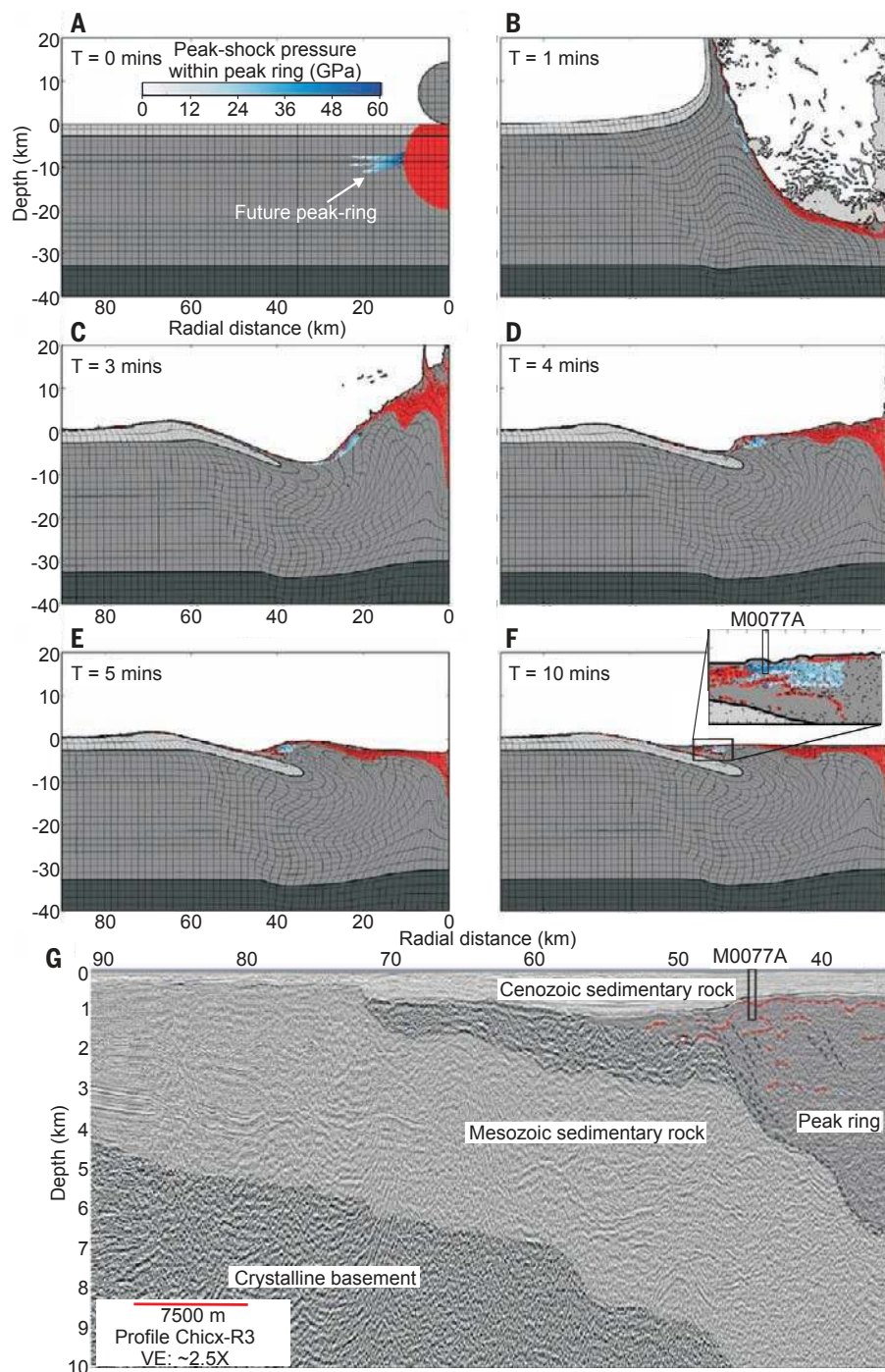


Fig. 1. Dynamic collapse model of peak-ring formation.

(A to F) Numerical simulation of the formation of Chicxulub (18) at 0, 1, 3, 4, 5, and 10 min tracking the material that eventually forms the peak ring [indicated by the arrow in (A)] and records the maximum shock pressure (blue color scale) to which the peak-ring rocks were exposed during passage of the shock wave. The red color indicates zones of impact melt, for which shock pressures have exceeded 60 GPa. The preimpact target rocks are composed of sediments (light gray), crust (medium gray), and mantle (dark gray). (G) Depth-converted, time-migrated seismic profile ChicxR3 (13). ChicxR3 is a radial profile (roughly west-northwest) that passes ~200 m from the location of M0077A. For comparison with the simulation, shading is added to match the final crater shown in (F), with light gray for inward-collapsed sedimentary rock, dark gray for peak-ring material, and white for Cenozoic sedimentary cover (21). Black dashed lines indicate dipping reflectors at the outer boundary of the peak ring, and red dashed lines mark reflectors that may be consistent with zones of impact melt rock in (F). IODP/ICDP Site M0077A is shown in (G) and placed in a similar position on the magnified inset of the model in (F). VE, vertical exaggeration.

from a number of exposed terrestrial impact structures supports the idea of dynamic collapse of the central uplift (9, 22–24) and that, in larger craters, the peak ring is formed from the interaction of two collapse regimes (25). In the simulation, the final crater (Fig. 1F) has the same key features as the upper 10 km of the Chicxulub crater, as imaged on a radial, depth-converted seismic reflection profile (Fig. 1G) (27). Specifically, a suite of dipping reflectors mark the boundary between Mesozoic sedimentary rocks and peak-ring rocks, with evidence of discrete melt zones within the peak ring (especially in the upper few hundred meters).

Before drilling, not all of the geophysical data appeared to be consistent with the hypothesis that the Chicxulub peak ring was formed from uplifted crustal basement. Gravity models and seismic refraction data indicated that the peak-ring rocks had a relatively low density ($2.2\text{--}2.3\text{ g cm}^{-3}$) (26) and seismic P wave velocity (3.9 to 4.5 km s^{-1}) (27). The seismic velocity of crustal basement rock outside the central crater is $>5.6\text{ km s}^{-1}$ (28), making it difficult to explain how crustal rocks

within the peak ring could have such a strongly reduced seismic velocity. The inferred physical properties have been explained by the peak ring being formed either from a thickened section of allochthonous impact breccia (26), which is a typical cover of crater floors, or from megabreccia (allochthonous breccia with large clasts $>10\text{ m}$), as seen in one of the annular rings at the Popigai impact structure in Siberia (8).

In April to May 2016, a joint effort by IODP and ICDP drilled the Chicxulub peak ring off-shore during Expedition 364 at site M0077A (21.45° N , 89.95° W) (Fig. 2A). The drill site is located at $\sim 45.6\text{ km}$ radial distance, using a previously selected nominal center for the Chicxulub structure of 21.30° N , 89.54° W (10). We recovered core between 505.7 and 1334.7 m below the seafloor (mbsf). We made visual descriptions through a transparent liner, while samples from the end of the core barrel (core catcher) were available for direct inspection. We made 114 smear slides and 51 thin sections from the core-catcher samples, which were taken at regular intervals

throughout the drill core. We measured petrophysical properties at the surface using a Multi-Sensor Core Logger (MSCL) and acquired a suite of wireline logging data from the seafloor to the bottom of the hole (21).

The upper part of the cored section from 505 to 618 mbsf consists of a sequence of hemipelagic and pelagic Paleogene sediments. We reached the top of the peak ring at 618 mbsf (Fig. 2, A and B). The uppermost peak ring is composed of $\sim 130\text{ m}$ of breccia, with impact melt fragments that overlie clast-poor impact melt rock (Fig. 2B). We encountered felsic basement rocks between 748 and 1334.7 mbsf that were intruded by preimpact mafic and felsic igneous dikes as well as impact-generated dikes. We recovered one particularly thick impact breccia and impact melt rock sequence between 1250 and 1316 mbsf. The entire section of felsic basement exhibits impact-induced deformation on multiple scales. There are many fractures (Fig. 3A), foliated shear zones (Fig. 3B), and cataclases (Fig. 3C), as well as signs of localized hydrothermal alteration (Fig. 3D). The felsic basement is

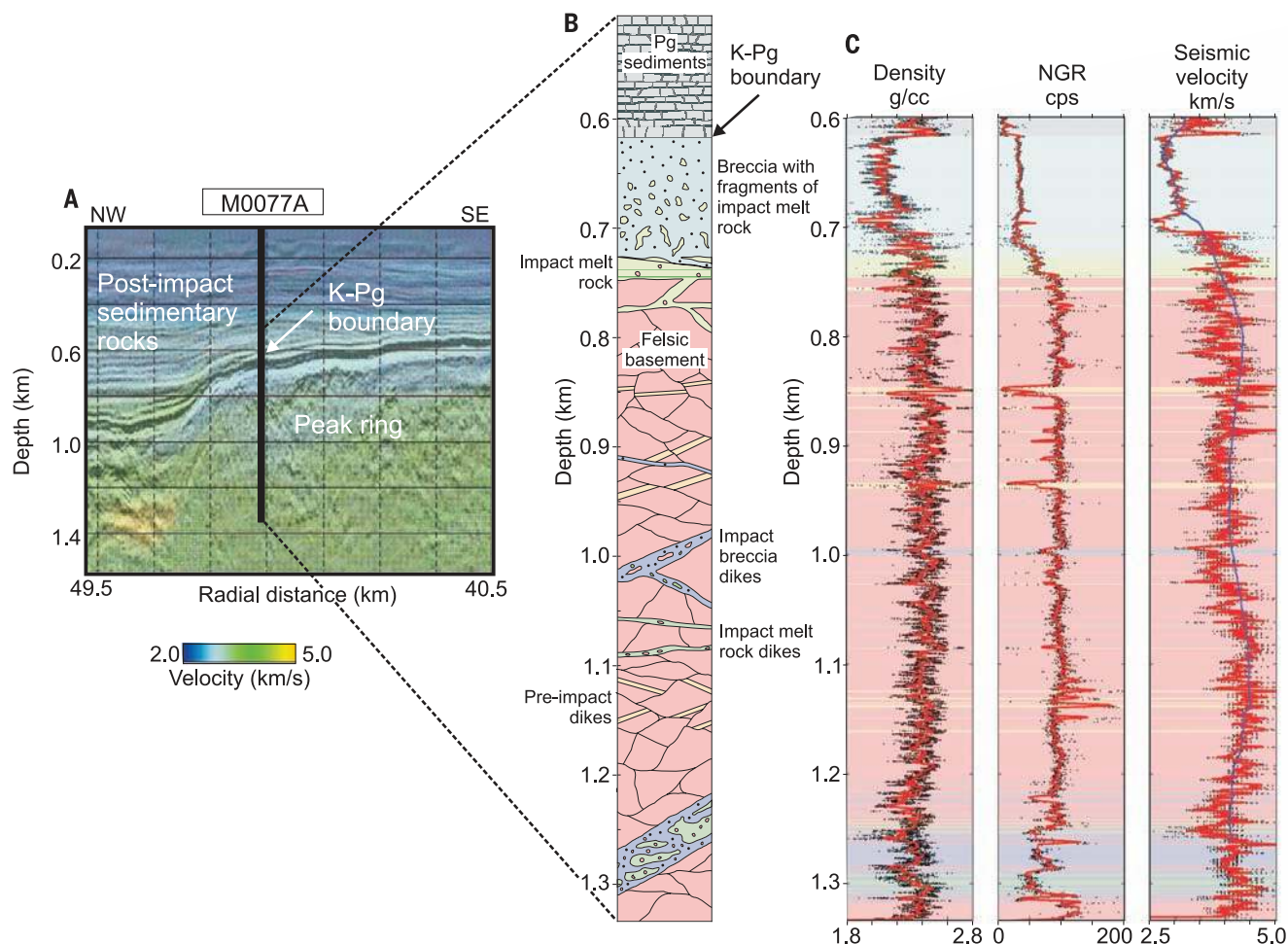


Fig. 2. IODP/ICDP Expedition 364. (A) Location of Site M0077A on depth-converted seismic reflection profile ChicxR3 (13, 14), overlain by seismic P wave velocity (27). (B) Lithology encountered at Site M0077A from 600 m to total depth, with Paleogene sediments (gray), breccia with impact melt fragments (blue), impact melt rock (green), felsic basement (pink), and preimpact dikes (yellow). In order to indicate a possible difference in origin, the blue and green color within the breccia is slightly lighter than in the dikes. (C) Corresponding petrophysical properties: gamma density [grams per cubic centimeter (g/cc)] and NGR [counts per second (cps)] measured on the cores using a MSCL, and seismic P wave velocity (km/s) obtained from sonic (red) and VSP (blue) wireline logging data (21).

predominantly a coarse-grained, roughly equigranular granitic rock (Fig. 3E) that is locally aplitic or pegmatitic and, in a few cases, syenitic. The basement rocks in the peak ring differ from basement in nearby drill holes encountered immediately below the Mesozoic sedimentary rocks, suggesting a source of origin that was deeper than 3 km (21).

In total, 18 of the smear slides and 17 of the thin sections were prepared from the felsic basement and viewed with an optical microscope. Evidence of shock metamorphism is pervasive throughout the entire basement, with quartz crys-

tals displaying up to four sets of decorated planar deformation features (Fig. 3F). We observed shatter cone fragments in preimpact dikes between 1129 and 1162 mbsf, as well as within the breccia (Fig. 3G). Jointly, the observed shock metamorphic features suggest that the peak ring rocks were subjected to shock pressures of ~10 to 35 GPa (29). No clear systematic variation in shock metamorphism was observed with depth. Impact melt, which is formed at shock pressures of >60 GPa, is also a component of the peak ring (Fig. 2B).

The formation of the Chicxulub peak ring from felsic basement (Fig. 2) confirms that crustal rocks

lie directly above Mesozoic sedimentary rocks (Fig. 1G), which is consistent with the dynamic collapse model of peak-ring formation (Fig. 1, A to F). On the contrary, the nested melt-cavity hypothesis does not predict this juxtaposition of units at the peak ring. In the numerical simulation shown in Fig. 1, the majority of the rocks that form the peak ring are subjected to peak-shock pressures in the 10 to 35 GPa range, with some zones of melt rock (Fig. 1, red), which is also consistent with our drill-core observations. Conversely, in the nested melt-cavity hypothesis, the peak-ring rocks are expected to be subjected to either higher (6) or lower average shock pressures (7) than we observed.

We investigated the physical properties of the peak-ring rocks using (i) core-based MSCL natural gamma ray (NGR) and gamma density logs and (ii) downhole sonic logs and vertical seismic profile (VSP) data that determine *P* wave velocity surrounding the borehole (Fig. 2C) (21). The drilling data confirm that the peak-ring rocks have low densities and seismic velocities, as suggested by geophysical models (26, 27). The density of the felsic basement varies between 2.10 and 2.55 g cm⁻³, with a mean of 2.41 g cm⁻³, and *P* wave velocities vary between 3.5 and 4.5 km s⁻¹, with a mean of 4.1 km s⁻¹. These values are unusually low for felsic basement, which typically has densities of >2.6 g cm⁻³ and seismic velocities of >5.5 km s⁻¹. We found that samples of the peak ring were variable in strength, locally quite hard, or friable. We also observed distinct variations in the rate of drill bit penetration over short distances (<1 m), with some sections seeming mechanically weaker than others. Fracturing, shock metamorphism, and other factors such as hydrothermal alteration may contribute to the reduction in seismic velocity and density of the felsic basement. Dilation during brittle deformation is observed in central uplifts in other large terrestrial impact craters (30, 31), and dilatancy is predicted to increase fracture porosity in the peak-ring rocks by between 1 and 5% (32). Shock metamorphism can also reduce density, as shown in experiments (33) and in nature (34).

One of the most enigmatic and enduring fundamental unknowns in impact cratering is how bowl-shaped transient cavities collapse to form larger, relatively flat final craters (1). To do so requires a temporary reduction in cohesive strength and internal friction (35, 36). In the model shown in Fig. 1, the rocks in the peak ring have moved a large distance (>20 km) during crater formation; hence, these units may well provide clues to the transient weakening mechanism that allows large craters to collapse.

The confirmation of the dynamic collapse model (Fig. 1, A to F) by the Expedition 364 results provides predictions about shock deformation, density reduction, and the kinematics of peak-ring formation. These predictions can be tested and refined through drill-core investigations of physical properties, paleomagnetism, structural data, and shock metamorphism. We anticipate improvement in constraints on impact energy and the sizes of the transient and excavation

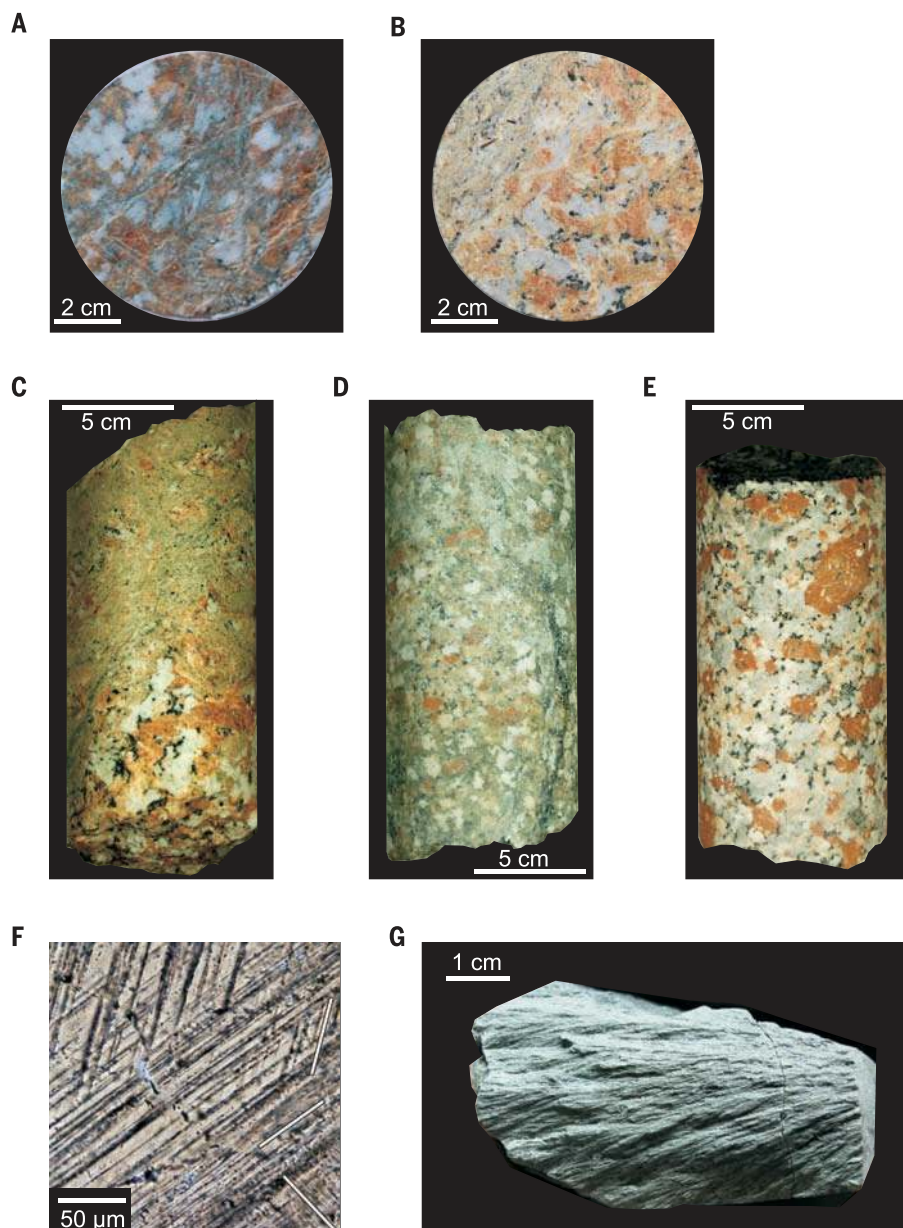


Fig. 3. Photographs from Expedition 364. (A to E) Felsic basement displaying (A) brittle faulting at 749.5 mbsf, (B) a foliated shear zone at 963.5 mbsf, (C) a cataclastic shear zone at 957.4 mbsf, (D) hydrothermal alteration at 930 mbsf, and (E) typical granitic basement with large crystals of red/brown potassium feldspar at 862.3 mbsf. (F) Shocked quartz from 826.9 mbsf in cross-polarized light, displaying three sets of planar deformation features (indicated by the solid white bars). (G) Shatter cone fragment from an amphibolite clast in the breccia at 708.5 mbsf.

cavities. As a consequence, the volumes of environmental pollutants released by the K-Pg impact will be better constrained, together with its role in causing the end-Cretaceous mass extinction (37). Because the deep subsurface biosphere is influenced by fracturing and mineralogical changes in host rocks induced by shock and post-impact hydrothermal activity, understanding how impact craters are formed and modify the environment will advance our understanding of deep subsurface life on Earth and potential habitability elsewhere.

The validation of the dynamic collapse model also strengthens confidence in simulations of large-crater formation on other planetary bodies. These simulations suggest that as crater size increases, the rocks that form peak rings originate from increasingly deeper depths (38). This relationship means that the composition of the peak-ring lithology provides information on the crustal composition and layering of planetary bodies and may be used to verify formation models, such as for the Moon (6, 38, 39). One of the principal observations used to support a version of the nested melt-cavity hypothesis in Baker *et al.* (7) is that peak rings within basins of all sizes on the Moon contain abundant crystalline anorthosite and must, therefore, originate from the upper crust, if indeed the lower crust is noritic. Our results suggest a deeper origin for peak-ring rocks and thus are more in accordance with alternative models for the composition of a heterogeneous lunar crust in which an anorthositic layer extends regionally to deeper depths (40, 41). The dynamic collapse model and Expedition 364 results predict density reduction through shock and shear fracturing within the uplifted material (33), which is consistent with the recent Gravity Recovery and Interior Laboratory (GRAIL) mission results of a highly porous lunar crust (42) and the presence of mid-crustal rocks juxtaposed by shear zones in the peak ring at the Schrödinger crater (38). This linkage between deformation and overturning of material at the scales >10 km implies that over an extended period of time, impact cratering greatly increases the porosity of the subsurface and causes vertical fluxes of materials within the crust.

REFERENCES AND NOTES

- H. J. Melosh, *Impact Cratering* (Oxford Univ. Press, 1989).
- W. S. Hale, R. A. F. Grieve, *J. Geophys. Res.* **87** (S01), A65 (1982).
- J. B. Murray, *Moon Planets* **22**, 269–291 (1980).
- J. S. Alexopoulos, W. B. McKinnon, *Spec. Pap. Geol. Soc. Am.* **293**, 29 (1994).
- M. J. Cintala, R. A. F. Grieve, *Meteorit. Planet. Sci.* **33**, 889–912 (1998).
- J. W. Head, *Geophys. Res. Lett.* **37**, L02203 (2010).
- D. M. H. Baker, J. W. Head, G. S. Collins, R. W. K. Potter, *Icarus* **273**, 146 (2016).
- P. M. Vermeesch, J. V. Morgan, *Meteorit. Planet. Sci.* **39**, 1019–1034 (2004).
- G. R. Osinski, J. G. Spray, *Meteorit. Planet. Sci.* **40**, 1813–1834 (2005).
- A. Camargo-Zanoguera, G. Suarez-Reynoso, *Bol. Asoc. Mex. Geof. Expl.* **34**, 1 (1994).
- J. V. Morgan *et al.*, *Nature* **390**, 471 (1997).
- A. R. Hildebrand *et al.*, *Spec. Publ. Geol. Soc. Lond.* **140**, 155 (1998).
- S. P. S. Gulick *et al.*, *Nat. Geosci.* **1**, 131–135 (2008).
- S. P. S. Gulick *et al.*, *Rev. Geophys.* **51**, 31–52 (2013).
- J. Brittan, J. Morgan, M. Warner, L. Marin, *Spec. Pap. Geol. Soc. Am.* **339**, 269 (1999).
- J. V. Morgan, M. R. Warner, G. S. Collins, H. J. Melosh, G. L. Christeson, *Earth Planet. Sci. Lett.* **183**, 347–354 (2000).
- B. Ivanov, *Sol. Syst. Res.* **39**, 381–409 (2005).
- G. S. Collins *et al.*, *Earth Planet. Sci. Lett.* **270**, 221–230 (2008).
- G. L. Christeson *et al.*, *Earth Planet. Sci. Lett.* **284**, 249–257 (2009).
- L. E. Senft, S. T. Stewart, *Earth Planet. Sci. Lett.* **287**, 471–482 (2009).
- Materials and methods are available as supplementary materials on Science Online.
- T. Kenkmann, I. von Dalwigk, *Meteorit. Planet. Sci.* **35**, 1189–1201 (2000).
- T. Kenkmann, G. S. Collins, K. Wünnemann, The modification stage of impact crater formation, *Impact Cratering* (Wiley-Blackwell, 2013).
- A. Jahn, U. Riller, *Spec. Pap. Geol. Soc. Am.* **518**, 85–97 (2015).
- R. A. F. Grieve, W. U. Reimold, J. Morgan, U. Riller, M. Pilkington, *Meteorit. Planet. Sci.* **43**, 855–882 (2008).
- M. Pilkington, A. Hildebrand, C. Ortiz-Aleman, *J. Geophys. Res.* **99** (E6), 13147 (1994).
- J. V. Morgan *et al.*, *J. Geophys. Res.* **116** (B6), B06303 (2011).
- G. Christeson, Y. Nakamura, R. T. Buffler, J. Morgan, M. Warner, *J. Geophys. Res.* **106** (B10), 21751–21769 (2001).
- R. A. F. Grieve, F. Langenhorst, D. Stöffler, *Meteorit. Planet. Sci.* **31**, 6–35 (1996).
- D. Lieger, U. Riller, R. L. Gibson, *Earth Planet. Sci. Lett.* **279**, 53–64 (2009).
- U. Riller, D. Lieger, R. L. Gibson, R. A. F. Grieve, D. Stöffler, *Geology* **38**, 619–622 (2010).
- G. S. Collins, *J. Geophys. Res.* **119**, 2600–2619 (2014).
- F. Langenhorst, A. Deutsch, *Earth Planet. Sci. Lett.* **125**, 407–420 (1994).
- A. C. Singleton, G. R. Osinski, P. J. A. McCausland, D. E. Moser, *Meteorit. Planet. Sci.* **46**, 1774–1786 (2011).
- H. J. Melosh, *Impact and Explosion Cratering* (Pergamon Press, 1977).
- W. B. McKinnon, *Lunar Planet. Sci. Conf. Proc.* **9**, 3965 (1978).
- P. R. Renne *et al.*, *Science* **339**, 684–687 (2013).
- D. A. Kring, G. Y. Kramer, G. S. Collins, *Nat. Commun.* **10**, 1038/ncomms13161 (2016).
- G. Y. Kramer, D. A. Kring, A. L. Nahm, C. M. Pieters, *Icarus* **223**, 131–148 (2013).
- S. Yamamoto *et al.*, *Geophys. Res. Lett.* **39**, L13201 (2012).
- T. Arai, H. Takeda, A. Yamaguchi, M. Ohtake, *Earth Planets Space* **60**, 433–444 (2008).
- M. A. Wieczorek *et al.*, *Science* **339**, 671–675 (2013).

ACKNOWLEDGMENTS

This research used samples and data provided by IODP. Samples can be requested at <http://web.iodp.tamu.edu/sdrmm> after the end of the moratorium on 19 October 2017. Expedition 364 was jointly funded by the European Consortium for Ocean Research Drilling (ECORD) and the International Continental Scientific Program, with contributions and logistical support from the Yucatan State Government and Universidad Nacional Autónoma de México (UNAM). G.S.C. was funded by UK Science and Technology Facilities Council grant ST/N000803/1. S.P.S.G. acknowledges his Fellowship at the Hanse-Wissenschaftskolleg, Germany. This is UTIG Contribution #3018.

SUPPLEMENTARY MATERIALS

www.sciencemag.org/content/354/6314/878/suppl/DC1
Material and Methods
Table S1
References (43–63)

27 July 2016; accepted 14 October 2016
10.1126/science.aah6561

ACTIVE MATTER

Command of active matter by topological defects and patterns

Chenhui Peng,* Taras Turiv,* Yubing Guo, Qi-Huo Wei, Oleg D. Lavrentovich†

Self-propelled bacteria are marvels of nature with a potential to power dynamic materials and microsystems of the future. The challenge lies in commanding their chaotic behavior. By dispersing swimming *Bacillus subtilis* in a liquid crystalline environment with spatially varying orientation of the anisotropy axis, we demonstrate control over the distribution of bacterial concentration, as well as the geometry and polarity of their trajectories. Bacteria recognize subtle differences in liquid crystal deformations, engaging in bipolar swimming in regions of pure splay and bend but switching to unipolar swimming in mixed splay-bend regions. They differentiate topological defects, heading toward defects of positive topological charge and avoiding negative charges. Sensitivity of bacteria to preimposed orientational patterns represents a previously unknown facet of the interplay between hydrodynamics and topology of active matter.

Swimming rodlike bacteria such as *Bacillus subtilis* show a distinct ability to sense and navigate their environment in search of nutrients. They propel in viscous fluids by rotating appendages called flagella, which are composed of bundles of thin helical filaments. Flagella can also steer the bacterium in a new direction by momentarily untangling the filaments and causing the bacterium to tumble (1). Alternat-

ing runs and tumbles of bacteria form a random trajectory reminiscent of a Brownian walk. The flows of the surrounding fluid created by bacteria cause their interactions and collective dynamics (2). Locally, the bacteria swim parallel to each other but globally this orientational order is unstable, showing seemingly chaotic patterns in both alignment of bacterial bodies and their velocities (3, 4). Similar out-of-equilibrium patterns are met in many other systems, universally called “active matter” and defined as collections of interacting self-propelled particles, each converting internally stored or ambient energy into a systematic movement and generating coordinated collective motion (5–7). To extract useful work from the

Liquid Crystal Institute and Chemical Physics Interdisciplinary Program, Kent State University, Kent, OH 44242, USA.

*These authors contributed equally to this work. †Corresponding author. Email: olavrent@kent.edu